

Electronic correlations and dynamical screening with *ab initio* quantum embedding

Chia-Nan Yeh,^{1,*} Francesco Petocchi,^{2,†} Alexander Hampel,^{1,‡} Philipp Werner,^{2,§}
Olivier Parcollet,^{1,3,¶} Antoine Georges,^{4,1,5,6,**} and Miguel Morales^{1,††}

¹*Center for Computational Quantum Physics, Flatiron Institute,
Simons Foundation, New York, NY 10010, USA*

²*Department of Physics, University of Fribourg, 1700 Fribourg, Switzerland*

³*Université Paris-Saclay, CNRS, CEA, Institut de Physique Théorique (IPhT), 91191 Gif-sur-Yvette, France*

⁴*Collège de France, 11 place Marcelin Berthelot, 75005 Paris, France*

⁵*CPHT, CNRS, École Polytechnique, Institut Polytechnique de Paris, Route de Saclay, 91128 Palaiseau, France*

⁶*Department of Quantum Matter Physics, University of Geneva,
24 Quai Ernest-Ansermet, 1211 Geneva 4, Switzerland*

(Dated: March 16, 2026)

First-principles descriptions of correlated quantum materials require a simultaneous treatment of strong local many-body effects and nonlocal dynamical screening. We present an efficient fully self-consistent implementation of GW +EDMFT that combines nonlocal effects at the GW level with a non-perturbative treatment of local correlations within extended dynamical mean-field theory (EDMFT), while providing a controlled double-counting prescription. Crucially, self-consistency in both the Green's function and the dynamically screened interaction is essential to achieve a consistent description of screening processes across energy scales. The efficient computation of this self-consistent solution is enabled here by compressing two-particle correlation functions using interpolative separable density fitting (ISDF). Applying the scheme to the Mott insulator SrMnO_3 and the correlated metal LaNiO_3 , we show that full self-consistency resolves the overscreening inherent to constrained-RPA approaches. By suppressing spurious low-energy screening channels, a Mott-insulating state in quantitative agreement with experiment is obtained for SrMnO_3 . These results establish fully self-consistent GW +EDMFT as a predictive *ab initio* framework for strongly correlated quantum materials.

Introduction—Accurate *ab initio* descriptions of quantum materials with strong electron correlations remain a central challenge in condensed matter physics. While density functional theory (DFT) offers a favorable balance between accuracy and cost, a universal functional capable of including strong correlation effects is not currently available. A many-body formalism, which also gives access to excited states, is therefore required.

A widely adopted strategy to incorporate many-body effects is *quantum embedding*. The general concept is to isolate, within the full Hilbert space \mathcal{B} of the material, a subspace \mathcal{C} spanned by correlated orbitals to which many-body methods are applied, while the remaining degrees of freedom $\mathcal{B}\setminus\mathcal{C}$ form an environment that is treated at a mean-field or perturbative level (Fig. 1).

Despite their conceptual simplicity, implementing quantum embedding strategies from first principles poses several major challenges. First, computing effective interactions for \mathcal{C} requires properly accounting for screening of the long-range Coulomb interaction, which involves processes associated with inter-band transitions in the full Hilbert space. In practice, perturbative approaches such as the constrained random phase approximation (cRPA) [1] are often used. cRPA is however known to lead to over-screening in models and materials [2–4]. The reason is illustrated in Figs. 1a-b: because cRPA is based on an inaccurate description of the correlated states in \mathcal{C} , contributions to the polarisation from transitions involving these states are overestimated. This is particularly evident in Mott insulators, in which \mathcal{C} states are pushed

away from zero-energy by the gap opening. Second, the double-counting (DC) contribution must be defined and removed consistently to ensure a consistent treatment of electronic correlations across Hilbert space partitions, a well-known issue when combining DFT with dynamical mean-field theory (DMFT) [5]. An improper treatment of the DC term leads for example to an incorrect relative energy between oxygen- p and metal- d states in transition-metal oxides. Finally, a self-consistent embedding scheme requires that the perturbative description of the \mathcal{B} space is updated in the presence of many-body corrections arising from \mathcal{C} , as done for example in charge self-consistent implementations of DFT+DMFT.

The combination of the GW approximation [6] and extended dynamical mean-field theory (EDMFT) [7–10], referred to as GW +EDMFT [11, 12], provides a promising theoretical framework for addressing these challenges. The method is formulated as an approximation within the Almladh free-energy functional framework, where many-body effects are encoded in the correlation functional $\Psi[G, W]$ of the interacting Green's function G and the screened interaction W (Fig. 1c):

$$\Psi[G, W] \approx \Psi_{\mathcal{B}}^{GW}[G, W] + \Psi_{\mathcal{C}}^{\text{EDMFT}}[G, W] - \Psi_{\mathcal{C}}^{\text{DC}}[G, W]. \quad (1)$$

Here $\Psi_{\mathcal{B}}^{GW}$ corresponds to the GW diagram across the entire \mathcal{B} space, incorporating long-range screening and non-local correlations. The *local* correlated subspace \mathcal{C} is treated non-perturbatively with EDMFT, identifying $\Psi_{\mathcal{C}}^{\text{EDMFT}}$ with the Almladh functional of a self-

consistent quantum impurity problem with dynamically screened interactions embedded in an effective non-interacting medium [11, 12] (Fig. 1c). The DC term Ψ_C^{DC} is defined as the local GW diagram which unambiguously removes contributions common to the first two terms.

Despite its conceptual appeal, fully self-consistent implementations of GW +EDMFT for real materials pose significant numerical challenges, owing to the high computational cost of achieving self-consistency in frequency-dependent two-particle quantities across the full \mathcal{B} space. Consequently, existing fully self-consistent studies have been largely restricted to model systems [13–16], while applications to realistic materials have relied on simplified schemes. These include quasiparticle GW combined with DMFT using static interactions derived from cRPA [17, 18], as well as variants that retain frequency-dependent impurity interactions but avoid full self-consistency, such as one-shot [19, 20] and multi-tier schemes [21, 22]. As a result, the physical consequences of a fully self-consistent GW +EDMFT treatment for real materials have remained largely unexplored, with only very recent work reporting such an implementation with applications to NiO and SrVO₃ [23].

In this article, we introduce an efficient implementation of fully self-consistent *ab initio* GW +EDMFT and demonstrate its successful application to two prototypical materials, a Mott insulator (SrMnO₃) and a correlated metal (LaNiO₃). We show that full self-consistency allows to overcome the issues emphasized above, most notably the overscreening problem, which otherwise prevents a correct description of the Mott insulator. Our GW +EDMFT implementation is made possible by recent advances in the compression of two-particle correlation functions based on interpolative separable density fitting (ISDF), which enable considerably more efficient self-consistent GW (sc GW) calculations with full frequency dependence [24–26]. Our work demonstrates the viability of GW +EDMFT as a first-principle electronic structure framework for materials with strong correlations.

Methods—We introduce a set of Kohn-Sham (KS) Bloch orbitals $\phi_i^{\mathbf{k}}(\mathbf{r})$ that spans the full Hilbert space \mathcal{B} . Here \mathbf{k} is a wave vector in the first Brillouin zone and i is the band index. The correlated subspace \mathcal{C} is defined via a projector $C_{ia}^{\mathbf{k}}$ onto a set of maximally localized Wannier functions (MLWFs), $w_a(\mathbf{r}) = \sum_{\mathbf{k}} \sum_i C_{ia}^{\mathbf{k}} \phi_i^{\mathbf{k}}(\mathbf{r})$, with $w_a(\mathbf{r})$ centered at the home unit cell. Crucially, an efficient implementation of sc GW requires a compact basis set for two-particle quantities. Instead of using the product basis set $\rho_{ij}^{\mathbf{k}\mathbf{k}-\mathbf{q}}(\mathbf{r}) = \phi_i^{\mathbf{k}^*}(\mathbf{r})\phi_j^{\mathbf{k}-\mathbf{q}}(\mathbf{r})$ we adopt the auxiliary basis $\zeta_{\mu}^{\mathbf{q}}(\mathbf{r})$ constructed using the ISDF method [24–26]:

$$\rho_{ij}^{\mathbf{k}\mathbf{k}-\mathbf{q}}(\mathbf{r}) \approx \sum_{\mu} \rho_{ij}^{\mathbf{k}\mathbf{k}-\mathbf{q}}(\mathbf{r}_{\mu}) \zeta_{\mu}^{\mathbf{q}}(\mathbf{r}) \quad (2)$$

Here \mathbf{r}_{μ} denotes the interpolation points, whose number controls the accuracy of the ISDF representation. At the

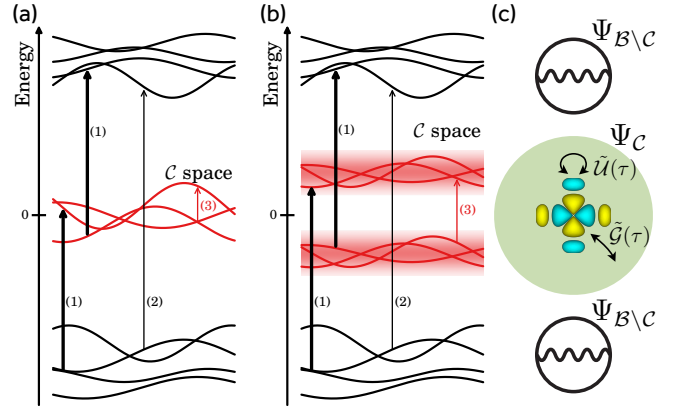


FIG. 1. (a) Different types of screening processes, involving transitions between \mathcal{B} and \mathcal{C} (1), within \mathcal{B} (2) and within \mathcal{C} (3). The cRPA construction removes processes of type (3) from the polarisation, keeping (1) and (2). (b) In a Mott insulator, a gap opens within \mathcal{C} . Self-consistent GW +EDMFT improves the description of screening processes of type (1) which remedies the overscreening problem of cRPA. (c) Perturbative and non-perturbative contributions to the Ψ functional in GW +EDMFT, within \mathcal{B} and \mathcal{C} respectively.

two-particle level, the mapping between \mathcal{B} and \mathcal{C} is performed using the projector $B_{ab\mu}^{\mathbf{q}}$, which expands the local Wannier product basis $w_a(\mathbf{r})w_b(\mathbf{r}) = \sum_{\mathbf{q}} \sum_{\mu} B_{ab\mu}^{\mathbf{q}} \zeta_{\mu}^{\mathbf{q}}(\mathbf{r})$ (for details, see Ref. [26]). In the following, a tilde indicates quantities expressed in the MLWF basis of \mathcal{C} .

The Green's function G and screened interaction W in the full Hilbert space, expanded in $\phi_i^{\mathbf{k}}(\mathbf{r})$ and $\zeta_{\mu}^{\mathbf{q}}(\mathbf{r})$ respectively, are related to the self-energy Σ and polarisation Π by the Dyson equations:

$$G_{ij}^{\mathbf{k}}(i\omega_n) = \left[G_0^{\mathbf{k},-1}(i\omega_n) - \Sigma^{\mathbf{k}}(i\omega_n) \right]_{ij}^{-1}, \quad (3a)$$

$$W_{\mu\nu}^{\mathbf{q}}(i\Omega_n) = \left[V^{\mathbf{q},-1} - \Pi^{\mathbf{q}}(i\Omega_n) \right]_{\mu\nu}^{-1}. \quad (3b)$$

Here $\omega_n = (2n + 1)\pi/\beta$ and $\Omega_n = 2n\pi/\beta$ ($n \in \mathcal{Z}$) are fermionic and bosonic Matsubara frequencies at inverse temperature β , while $G_0^{\mathbf{k}}$ and $V^{\mathbf{q}}$ are the non-interacting Green's function and the bare Coulomb interaction. For simplicity, we will omit frequency arguments and basis indices when unambiguous.

Given the interacting propagators G and W , the self-energy and polarization are obtained from the functional derivatives $\Sigma = \delta\Psi/\delta G$ and $\Pi = -2, \delta\Psi/\delta W$. Within GW +EDMFT, these take the form [12]:

$$\Sigma^{\mathbf{k}} = \Sigma_{GW}^{\mathbf{k}} + C^{\mathbf{k}\dagger} \left[\tilde{\Sigma}_{\text{imp}} - \tilde{\Sigma}_{\text{DC}} \right] C^{\mathbf{k}}, \quad (4a)$$

$$\Pi^{\mathbf{q}} = \Pi_{GW}^{\mathbf{q}} + B^{\mathbf{q}\dagger} \left[\tilde{\Pi}_{\text{imp}} - \tilde{\Pi}_{\text{DC}} \right] B^{\mathbf{q}}. \quad (4b)$$

The GW contributions $\Sigma_{GW}^{\mathbf{k}}$ and $\Pi_{GW}^{\mathbf{q}}$ are evaluated in the full Hilbert space \mathcal{B} using a cubic-scaling algorithm within the ISDF formalism [26]. The corresponding DC terms $\tilde{\Sigma}_{\text{DC}} = \tilde{G}_{\text{loc}} \tilde{W}_{\text{loc}}$ and $\tilde{\Pi}_{\text{DC}} = \tilde{G}_{\text{loc}} \tilde{G}_{\text{loc}}$

represent the same GW diagrams evaluated using the local projected propagators within the \mathcal{C} space, $\tilde{G}_{\text{loc}} = \sum_{\mathbf{k}} C^{\mathbf{k}} G^{\mathbf{k}} C^{\mathbf{k}\dagger}$ and $\tilde{W}_{\text{loc}} = \sum_{\mathbf{q}} B^{\mathbf{q}} W^{\mathbf{q}} B^{\mathbf{q}\dagger}$.

The impurity self-energy $\tilde{\Sigma}_{\text{imp}}$ and polarization $\tilde{\Pi}_{\text{imp}}$ are obtained by solving an EDMFT impurity problem defined by the fermionic and bosonic Weiss fields $\tilde{G}^{-1}(i\omega_n) = \tilde{G}_{\text{loc}}^{-1}(i\omega_n) + \tilde{\Sigma}_{\text{imp}}(i\omega_n)$ and $\tilde{U}^{-1}(i\Omega_n) = \tilde{W}_{\text{loc}}^{-1}(i\Omega_n) + \tilde{\Pi}_{\text{imp}}(i\Omega_n)$ using a numerically exact continuous-time quantum Monte Carlo impurity solver [27, 28]. The EDMFT corrections $\tilde{\Sigma}_{\text{imp}} - \tilde{\Sigma}_{\text{DC}}$ and $\tilde{\Pi}_{\text{imp}} - \tilde{\Pi}_{\text{DC}}$ are then upfolded to the full Hilbert space \mathcal{B} using the projectors $C^{\mathbf{k}}$ and $B^{\mathbf{q}}$.

The lattice Green's function $G^{\mathbf{k}}$ and screened interaction $W^{\mathbf{q}}$ are updated using the resulting $\Sigma^{\mathbf{k}}$ and $\Pi^{\mathbf{q}}$, which completes one iteration of the self-consistent cycle. The procedure is iterated until the locally projected propagators coincide with the impurity Green's function and screened interaction, $\tilde{G}_{\text{loc}} = \tilde{G}_{\text{imp}}$ and $\tilde{W}_{\text{loc}} = \tilde{W}_{\text{imp}}$.

Results—We assess the performance of self-consistent GW +EDMFT by studying two prototypical materials: the Mott insulator SrMnO_3 and the correlated metal LaNiO_3 . SrMnO_3 crystallizes in the ideal cubic perovskite structure (space group $Pm\bar{3}m$). In the high-temperature cubic phase, Mn is in a $t_{2g}^3 e_g^0$ configuration and the system is a paramagnetic insulator; upon cooling, G-type antiferromagnetic order sets in below ~ 260 K. Photoemission experiments reveal an insulating gap, even above $T_{\text{Néel}}$, and reveal a valence band dominated by Mn- t_{2g} and O- $2p$ states, together with a conduction band of predominantly Mn- e_g character [29–31]. LaNiO_3 is the only rare-earth nickelate of the RNiO_3 family that remains metallic down to low temperature. It is often described as close to cubic, adopting a rhombohedrally distorted perovskite structure ($R\bar{3}c$) in which modest octahedral rotations reduce the symmetry from $Pm\bar{3}m$. The Ni ions are in a low-spin $t_{2g}^6 e_g^1$ configuration in a negative charge-transfer regime, yielding a strongly correlated metal with substantial Ni- $3d$ /O- $2p$ hybridization and a narrow band with predominantly e_g character at the Fermi level. Consistent with this picture, experiments report sizeable mass enhancements and proximity to charge and spin instabilities [32, 33].

All calculations are carried out on a $10 \times 10 \times 10$ k -mesh at inverse temperature $\beta = 15$ eV $^{-1}$. The \mathcal{B} space is spanned by KS orbitals constructed using **Quantum ESPRESSO** [34]. The GW +EDMFT self-consistency loop is initialized from a fully converged scGW solution. The correlated space \mathcal{C} is defined by transition-metal $3d$ MLWFs obtained with **Wannier90** [35] from an isolated low-energy window with predominantly $3d$ character. The resulting Wannier orbitals retain a finite O- $2p$ component, reflecting substantial transition-metal–oxygen covalency.

For each compound we perform two GW +EDMFT calculations corresponding to different \mathcal{C} spaces. (i) In the first scheme, we consider the bands closest to the Fermi level, obtaining a minimal correlated space consisting of the Mn- t_{2g} orbitals in SrMnO_3 (\mathcal{C}_3) and the Ni- e_g orbitals in LaNiO_3 (\mathcal{C}_2). (ii) In the second scheme we re-

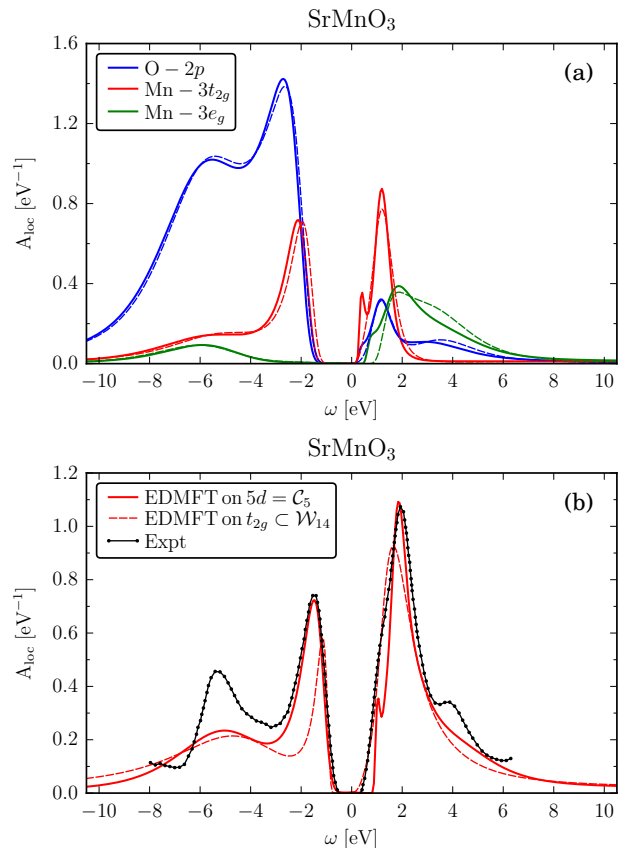


FIG. 2. (a) Local GW +EDMFT spectral functions for SrMnO_3 . The EDMFT space is either the full Mn- $3d$ shell defined by \mathcal{C}_5 (thick lines) or the Mn- t_{2g} states of \mathcal{C}_3 (dashed lines). For a fair comparison of both cases, the spectral functions are projected on the same set of very localized Wannier orbitals of \mathcal{W}_{14} . (b) Comparison to experimental PES and XAS data from Ref. 31 (black dots). Thick lines correspond to calculations in which the full Mn $3d$ shell is included in the EDMFT impurity problem (same curve of the upper panel), while dashed lines denote a minimal Mn- t_{2g} EDMFT submanifold extracted from \mathcal{W}_{14} .

tain within EDMFT the entire transition metal $3d$ shell of the correlated space \mathcal{C}_5 . This approach enables us to assess the robustness of the GW +EDMFT results with respect to the choice of correlated orbitals defining \mathcal{C} . To compare the spectral properties of these two schemes on equal footing, we project the converged spectral functions on a common set of very localized Wannier states obtained from a large energy window that includes the O- $2p$ states, labeled by \mathcal{W}_{14} .

In Fig. 2 we report the local spectral functions for SrMnO_3 . The GW +EDMFT method converges to a paramagnetic Mott insulating state. This is a remarkable result, since previous multi-tier calculations, relying on a single-shot G^0W^0 description of the high-energy states, failed to obtain an insulating solution in the paramagnetic phase [22, 36]. This is because the

DFT G_0 on which the calculation of W_0 is based has d -states at the Fermi level, while these states are in reality located in lower and upper Hubbard bands away from the Fermi level, hence leading to a much weaker screening, as illustrated in Fig. 1a-b. When full self-consistency is achieved, this effect is properly taken into account by GW +EDMFT, hence correcting the over-screening problem. This result highlights the ability of GW +EDMFT to properly describe spectral properties and screening in Mott insulators. In Fig. 2b, we compare the GW +EDMFT spectrum to photoemission (PES) ($\omega < 0$) and XAS ($\omega > 0$) experiments [31] (black dotted lines). The XAS intensity predominantly reflects the unoccupied $3d$ -derived density of states via $2p$ - $3d$ hybridization and hence the onset and overall profile of the XAS spectrum provide a reasonable experimental proxy for the unoccupied part of the local spectral function. Our results for the insulating gap and spectra compare quite well to experiments. Note that the experimental intensity of the peak at ~ -5.5 eV may be quite sensitive to the procedure used in Ref. [31] to separate the contribution of the Mn $3d$ -states from that of other states.

To test the robustness of the embedding scheme, we performed an additional calculation in which the minimal three orbital Mn- t_{2g} EDMFT subspace is constructed from a larger energy window containing also the oxygen states. This corresponds to quite localized atomic-like correlated orbitals to which non-perturbative many-body effects are applied within EDMFT, as commonly done also in some static implementations of DMFT [37]. The resulting EDMFT problem and the treatment of the oxygen states is the same as in previous multi-tier studies [21, 22], with the crucial improvement that in the present work the EDMFT self-energy is upfolded to the full space and the latter is treated at the scGW level.

The local spectral functions obtained from this scheme, shown in Fig. 2b (dashed lines), are in excellent agreement with both the converged results obtained using the other embedding and downfolding choice and with the experimental data (right panel). This demonstrates that our scheme yields internally consistent solutions for different choices of correlated manifolds.

In Fig. 3, we display the LaNiO₃ local spectral functions obtained from GW +EDMFT with a correlated space corresponding to either the full Ni- $3d$ shell \mathcal{C}_5 , or the e_g subset \mathcal{C}_2 . The calculations yield consistent spectra characterized by occupied t_{2g} orbitals and a quasiparticle peak with predominantly e_g character. The results are consistent with a metal with intermediate electronic correlations.

As a general trend, we observe that the spectral functions associated with the manifolds that are *always* treated within EDMFT, namely the Mn- t_{2g} states for SrMnO₃ (dashed red lines of Fig. 2) and the Ni- e_g states for LaNiO₃ (dashed green lines of Fig. 3), are not significantly modified when the impurity model is enlarged from either \mathcal{C}_3 or \mathcal{C}_2 to the full $3d$ shell \mathcal{C}_5 (thick red and green lines). For the cases at hand, this is expected be-

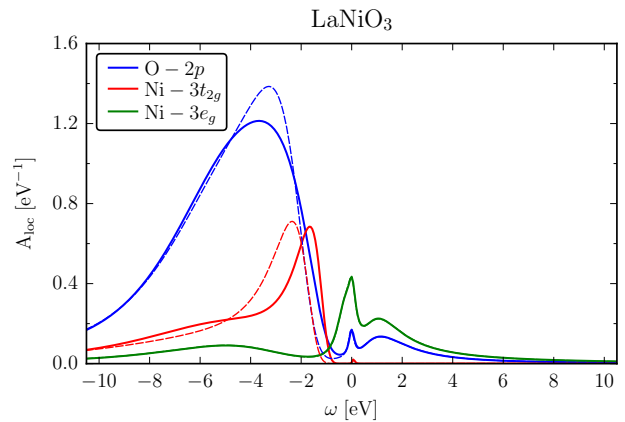


FIG. 3. Local GW +EDMFT spectral functions for LaNiO₃ downfolded to MLWFs projected onto MLWFs constructed from a large energy window. Thick and dashed lines correspond respectively to the case where EDMFT encompasses the full Ni- $3d$ from \mathcal{C}_5 and minimal Ni- e_g from \mathcal{C}_2 .

cause the excluded orbitals are either nearly empty (Mn- e_g) or nearly filled (Ni- t_{2g}) thus justifying *both* minimal and full- $3d$ embeddings. This is expected to be material-dependent and not a universal result, however: a physically motivated approach is to include in the subspace \mathcal{C} treated with EDMFT all the MLWFs with fractional filling, whose exclusion would omit important inter-orbital correlations.

In Fig. 4 we show the local dynamical interactions for the Mn- t_{2g} and Ni- e_g MLWFs. The top panels display in black the local cRPA interaction computed from G_0W_0 , and in red the effective local interaction $\mathcal{U}^{GW+EDMFT}$ obtained from the converged GW +EDMFT calculation. A first important observation is that, in the low-frequency regime, \mathcal{U} is systematically larger than the cRPA prediction. This reflects the above-mentioned overscreening of cRPA, which is based on the DFT bandstructure. When the self-energy modifies the low-energy electronic structure, screening processes are suppressed, resulting in a larger effective interaction. Note that the relative enhancement of the static interaction is stronger in the Mott insulating SrMnO₃ than in the correlated metal LaNiO₃. Once strong correlations are accounted for, the frequency dependence of \mathcal{U} becomes less pronounced than that of U^{cRPA} and the high-frequency limit is essentially given by scGW. A relevant observation is that the low-frequency limit of \mathcal{U} is quantitatively consistent with the (empirical) static Hubbard U parameters commonly used in DFT+DMFT studies of these two compounds. Specifically, \mathcal{U} yields local interactions of 3-5 eV for SrMnO₃ and 4-6 eV for LaNiO₃, which is close to the typical DFT+DMFT parameters: typically $U = 2.5$ -5 eV with $J = 0.5$ -0.7 eV for Mn [38-42], and $U = 5$ -7 eV with $J = 0.7$ -1 eV for Ni [43-49].

The local polarizations shown in the insets of Fig. 4 reveal a clear system-dependent contrast between the

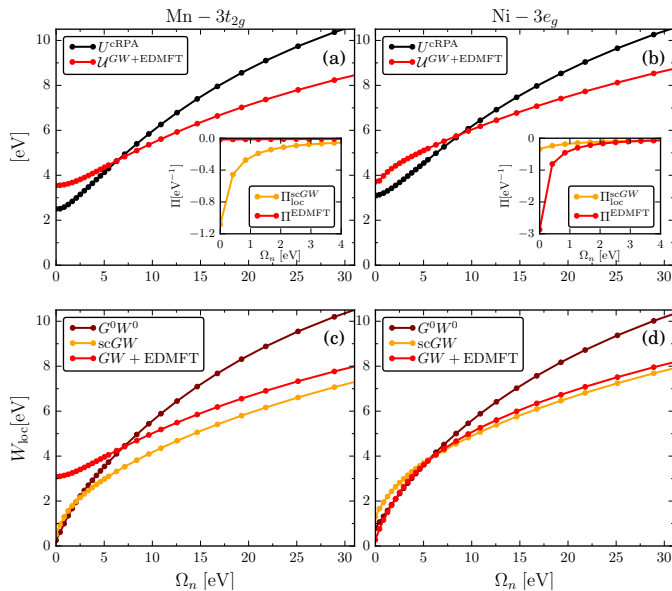


FIG. 4. Local interactions for Mn- t_{2g} and Ni- e_g Wannier orbitals defined in the full $3d$ correlated manifold. Top panels report the local cRPA interaction and the effective local interactions U^{GW} and U^{EDMFT} of the scGW and GW+EDMFT converged solutions respectively. The inset shows the local EDMFT polarization compared to the corresponding RPA one. Bottom panels report the local bosonic propagators where electronic correlations are treated within perturbation theory and GW+EDMFT. Quantities plotted with yellow and red lines are linked through the same local Dyson equation.

perturbative scGW estimate $\Pi_{\text{loc}}^{\text{scGW}}$ and the local GW+EDMFT polarization Π^{EDMFT} . For SrMnO₃, the RPA-like polarization, indicated by a yellow curve, displays a strongly metallic behavior missing the Mott-insulating ground state, whereas the EDMFT impurity polarization in red is smaller by several orders of magnitude, reflecting the strong suppression of local charge fluctuations. In metallic LaNiO₃, by contrast, the difference between the two polarizations is more moderate, but interestingly Π^{EDMFT} is larger than the perturbative estimate, indicating enhanced local charge fluctuations captured by GW+EDMFT. Taken together, these results highlight the limitations of purely perturbative approaches in the moderate to strong correlation regimes.

We note that both $W^{G^0W^0}$ and U^{cRPA} display a strong frequency dependence over the displayed frequency range. In contrast, self-consistency considerably weakens this frequency dependence, both at the GW and GW+EDMFT levels. At low frequencies, W^{scGW} generally exhibits an *increase* relative to $W^{G^0W^0}$, a trend that appears in both materials but is more pronounced for metallic LaNiO₃. This behavior indicates that scGW underestimates screening effects at low energies in correlated metals. This observation is consistent with the tendency of scGW to overestimate band gaps in semiconductors compared to single-shot G^0W^0 . Once the EDMFT correction is included, the contrast between

metallic LaNiO₃ and insulating SrMnO₃ becomes evident. In LaNiO₃, the GW+EDMFT screened interaction smoothly interpolates between the high-energy behavior of W^{scGW} and the low-energy behavior of $W^{G^0W^0}$, with a crossover around 5 eV. In contrast, the GW+EDMFT bosonic propagator for insulating SrMnO₃ differs dramatically from any perturbative result: both $W^{G^0W^0}$ and W^{scGW} severely underestimate the magnitude of the screened interaction over a broad frequency range. The GW+EDMFT screened interaction instead approaches the effective local interaction U^{EDMFT} from below.

These observations lead to two main conclusions: (i) strong local correlations are beyond the reach of perturbative approaches, which hence systematically underestimate the screened interaction in Mott insulators; and (ii) in the Mott-insulating state, local charge fluctuations are strongly suppressed, resulting in a small impurity polarization. As a consequence, the fully screened interaction W of a Mott insulator remains close to the local effective interaction U .

Conclusion— We demonstrated that fully self-consistent GW+EDMFT [11, 12, 23] provides a controlled, parameter-free quantum embedding description of electronic correlations and screening in real materials, with a well-defined double-counting correction and a self-consistently determined impurity interaction. Applying this framework to prototypical correlated perovskites, we find that self-consistency stabilizes a Mott-insulating solution in good agreement with photoemission data for cubic SrMnO₃, and reveals significant deviations from the local RPA polarization in LaNiO₃. In the Mott insulating system, charge fluctuations are strongly suppressed due to non-perturbative vertex corrections, leading to an effective local interaction that is substantially larger and less structured than predicted by cRPA. In metallic LaNiO₃ charge fluctuations are instead enhanced by correlation effects. Comparing minimal and full- $3d$ correlated manifolds yields similar low-energy spectra for the correlated subspaces in both compounds, highlighting the robustness of the method with respect to the choice of the correlated space. The efficient realization of these fully self-consistent calculations is enabled by compressing two-particle correlation functions using ISDF. These results establish self-consistent GW+EDMFT as a practical *ab initio* framework and motivate applications to systems in which the interplay of screening, covalency, and strong correlations governs metal-insulator transitions, non-Fermi liquid behavior, and other many-body phenomena.

ACKNOWLEDGMENTS

We are grateful to Sangkook Choi, Gabriel Kotliar, Jernej Mravlje, Malte Rösner and Nils Wentzell for useful discussions. F.P. acknowledges the support of the University of Geneva and of the Simons Foundation. The Flatiron Institute is a division of the Simons Foundation.

- * This author contributed equally to this work.;
 cyeh@flatironinstitute.org
- † This author contributed equally to this work.;
 francesco.petocchi@unifr.ch
- ‡ mail@alexander-hampel.de
- § philipp.werner@unifr.ch
- ¶ olivier.parcollet@cea.fr
- ** ageorges@flatironinstitute.org
- †† mmorales@flatironinstitute.org
- [1] F. Aryasetiawan, M. Imada, A. Georges, G. Kotliar, S. Biermann, and A. I. Lichtenstein, *Phys. Rev. B* **70**, 195104 (2004).
- [2] B. Amadon, T. Applencourt, and F. Bruneval, *Phys. Rev. B* **89**, 125110 (2014).
- [3] H. Shinaoka, M. Troyer, and P. Werner, *Phys. Rev. B* **91**, 245156 (2015).
- [4] C. Honerkamp, H. Shinaoka, F. F. Assaad, and P. Werner, *Phys. Rev. B* **98**, 235151 (2018).
- [5] K. Haule, *Phys. Rev. Lett.* **115**, 196403 (2015).
- [6] L. Hedin, *Phys. Rev.* **139**, A796 (1965).
- [7] A. M. Sengupta and A. Georges, *Phys. Rev. B* **52**, 10295 (1995).
- [8] Q. Si and J. L. Smith, *Phys. Rev. Lett.* **77**, 3391 (1996).
- [9] J. L. Smith and Q. Si, *Phys. Rev. B* **61**, 5184 (2000).
- [10] R. Chitra and G. Kotliar, *Phys. Rev. Lett.* **84**, 3678 (2000).
- [11] P. Sun and G. Kotliar, *Phys. Rev. B* **66**, 085120 (2002).
- [12] S. Biermann, F. Aryasetiawan, and A. Georges, *Phys. Rev. Lett.* **90**, 086402 (2003).
- [13] T. Ayrál, P. Werner, and S. Biermann, *Phys. Rev. Lett.* **109**, 226401 (2012).
- [14] T. Ayrál, S. Biermann, and P. Werner, *Phys. Rev. B* **87**, 125149 (2013).
- [15] P. Hansmann, T. Ayrál, L. Vaugier, P. Werner, and S. Biermann, *Phys. Rev. Lett.* **110**, 166401 (2013).
- [16] R. Sakuma, P. Werner, and F. Aryasetiawan, *Phys. Rev. B* **88**, 235110 (2013).
- [17] J. M. Tomczak, *Journal of Physics: Conference Series* **592**, 012055 (2015).
- [18] S. Choi, A. Kutepov, K. Haule, M. van Schilfhaarde, and G. Kotliar, *npj Quantum Materials* **1**, 16001 (2016).
- [19] J. M. Tomczak, M. Casula, T. Miyake, F. Aryasetiawan, and S. Biermann, *Europhysics Letters* **100**, 67001 (2012).
- [20] J. M. Tomczak, M. Casula, T. Miyake, and S. Biermann, *Phys. Rev. B* **90**, 165138 (2014).
- [21] F. Nilsson, L. Boehnke, P. Werner, and F. Aryasetiawan, *Phys. Rev. Mater.* **1**, 043803 (2017).
- [22] R. Mushkaev, F. Petocchi, V. Christiansson, and P. Werner, *npj Comput. Mater.* **10**, 182 (2024).
- [23] B. Kang, P. Semon, C. Melnick, M. Han, S. Mo, H. Lee, G. Kotliar, and S. Choi, *Computer Physics Communications* **308**, 109447 (2025).
- [24] J. Lu and L. Ying, *J. Comput. Phys.* **302**, 329 (2015).
- [25] C.-N. Yeh and M. A. Morales, *Journal of Chemical Theory and Computation* **19**, 6197 (2023).
- [26] C.-N. Yeh and M. A. Morales, *Journal of Chemical Theory and Computation* **20**, 3184 (2024).
- [27] P. Werner and A. J. Millis, *Phys. Rev. Lett.* **104**, 146401 (2010).
- [28] N. Kavokine, H. Lu, T. Ayrál, M. Ferrero, N. Wentzell, and O. Parcollet, *Journal of Open Source Software* **10**, 7425 (2025).
- [29] T. Saitoh, A. E. Bocquet, T. Mizokawa, H. Namatame, A. Fujimori, M. Abbate, Y. Takeda, and M. Takano, *Phys. Rev. B* **51**, 13942 (1995).
- [30] J.-S. Kang, H. J. Lee, G. Kim, D. H. Kim, B. Dabrowski, S. Kolesnik, H. Lee, J.-Y. Kim, and B. I. Min, *Phys. Rev. B* **78**, 054434 (2008).
- [31] D. H. Kim, H. J. Lee, B. Dabrowski, S. Kolesnik, J. Lee, B. Kim, B. I. Min, and J.-S. Kang, *Phys. Rev. B* **81**, 073101 (2010).
- [32] H. Guo, Z. W. Li, L. Zhao, Z. Hu, C. F. Chang, C.-Y. Kuo, W. Schmidt, A. Piovano, T. W. Pi, O. Sobolev, D. I. Khomskii, L. H. Tjeng, and A. C. Komarek, *Nature Communications* **9**, 10.1038/s41467-017-02524-x (2018).
- [33] Y. Shin and J. M. Rondinelli, *Phys. Rev. Res.* **4**, L022069 (2022).
- [34] P. Giannozzi, O. Baseggio, P. Bonfà, D. Brunato, R. Car, I. Carnimeo, C. Cavazzoni, S. de Gironcoli, P. Delugas, F. F. Ruffino, A. Ferretti, N. Marzari, I. Timrov, A. Urru, and S. Baroni, *J. Chem. Phys.* **152**, 154105 (2020).
- [35] A. A. Mostofi, J. R. Yates, G. Pizzi, Y.-S. Lee, I. Souza, D. Vanderbilt, and N. Marzari, *Computer Physics Communications* **185**, 2309 (2014).
- [36] F. Petocchi, F. Nilsson, F. Aryasetiawan, and P. Werner, *Phys. Rev. Res.* **2**, 013191 (2020).
- [37] G. Kotliar, S. Y. Savrasov, K. Haule, V. S. Oudovenko, O. Parcollet, and C. A. Marianetti, *Rev. Mod. Phys.* **78**, 865 (2006).
- [38] J. Mravlje, M. Aichhorn, and A. Georges, *Phys. Rev. Lett.* **108**, 197202 (2012).
- [39] H. Chen, H. Park, A. J. Millis, and C. A. Marianetti, *Phys. Rev. B* **90**, 245138 (2014).
- [40] D. Bauernfeind, R. Triebel, M. Zingl, M. Aichhorn, and H. G. Evertz, *Phys. Rev. B* **97**, 115156 (2018).
- [41] C. Ricca, I. Timrov, M. Cococcioni, N. Marzari, and U. Aschauer, *Phys. Rev. B* **99**, 094102 (2019).
- [42] O. Y. Long, G. Sai Gautam, and E. A. Carter, *Phys. Rev. Mater.* **4**, 045401 (2020).
- [43] X. Deng, M. Ferrero, J. Mravlje, M. Aichhorn, and A. Georges, *Phys. Rev. B* **85**, 125137 (2012).
- [44] O. E. Peil, M. Ferrero, and A. Georges, *Phys. Rev. B* **90**, 045128 (2014).
- [45] A. Subedi, O. E. Peil, and A. Georges, *Phys. Rev. B* **91**, 075128 (2015).
- [46] E. A. Nowadnick, J. P. Ruf, H. Park, P. D. C. King, D. G. Schlom, K. M. Shen, and A. J. Millis, *Phys. Rev. B* **92**, 245109 (2015).
- [47] H. Park, A. J. Millis, and C. A. Marianetti, *Phys. Rev. B* **93**, 235109 (2016).
- [48] X. Liao, V. Singh, and H. Park, *Phys. Rev. B* **103**, 085110 (2021).
- [49] U. Herath, S. S. Bhat, V. Singh, A. T. Lee, A. T. Ngo, H. Park, and A. H. Romero, *J. Phys. Chem. C* **130**, 977 (2026).